Development of a MEMS Microvalve Array for Fluid Flow Control

Nelsimar Vandelli, Donald Wroblewski, Margo Velonis, and Thomas Bifano

Abstract— **A microelectromechanical system (MEMS) microvalve array for fluid flow control is described. The device consists of a parallel array of surface-micromachined binary microvalves working cooperatively to achieve precision flow control on a macroscopic level. Flow rate across the microvalve array is proportional to the number of microvalves open, yielding a scalable high-precision fluidic control system.**

Device design and fabrication, using a one-level polycrystalline silicon surface-micromachining process combined with a single anisotropic bulk etching process are detailed. Performance measurements on fabricated devices confirm feasibility of the fluidic control concept and robustness of the electromechanical design. Air-flow rates of 150 ml/min for a pressure differential of 10 kPa were demonstrated. Linear flow control was achieved over a wide range of operating flow rates.

A continuum fluidic model based on incompressible low Reynolds number flow theory was implemented using a finite-difference approximation. The model accurately predicted the effect of microvalve diaphragm compliance on flow rate. Excellent agreement between theoretical predictions and experimental data was obtained over the entire range of flow conditions tested experimentally. [351]

I. Introduction

THE POTENTIAL for precise control of fluid flow on a small scale has motivated the development of silicon-micromachined microvalves and micropumps using microelectromechanical system (MEMS) technology. Such devices are potentially important in applications that include biomedical dosing, biochemical reaction systems, and microfluidic mixing and regulation. In the work described here, microfluidic devices consisting of parallel arrays of surface-micromachined microvalves have been designed, fabricated, and tested. Such devices are capable of precise regulation of flow across a silicon-based chip and exhibit a linear scalable valve function over a wide range of flow rates.

Microvalve arrays differ fundamentally in performance from single-channel-micromachined flow control valves for which the flow rate is controlled by varying the size of a single flow channel. Flow rate through a microvalve array scales linearly with the number of microvalves open, whereas flow rate through a single-channel valve varies, in low Reynolds number flows, with the cube of channel height [1], [2]. Moreover, array systems achieve precise flow control by relying on multiplicity of simple low-precision elements rather than a single more complex high-precision element. This offers an advantage in fabrication since in micromachining, multiplicity has a relatively low cost while complexity has a relatively high cost.

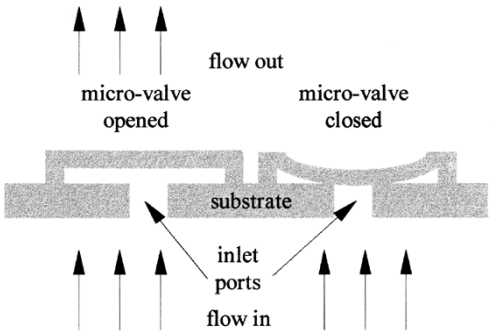

Fig. 1. Microvalve array conceptual design. To modulate flow, a voltage is applied between the microvalve diaphragm and substrate, causing the diaphragm to collapse unstably into contact with the substrate, thereby closing the inlet port and restricting flow.

Each microvalve is an independently controlled binary actuator consisting of a surface-micromachined diaphragm fixed along two sides [3]. The diaphragm is positioned over an inlet port anisotropically etched in a silicon substrate. The microvalve operates as a parallel plate electrostatic actuator with the diaphragm functioning as the moving electrode and the silicon substrate as the ground electrode. If a voltage is applied between the diaphragm and the substrate, an electrostatic force develops, causing the diaphragm to deflect toward the substrate. At any applied voltage, diaphragm equilibrium is achieved as a balance between electrostatic force and diaphragm mechanical restoring force. As the voltage increases, the diaphragm experiences electromechanical instability and collapses spontaneously toward the substrate, closing the inlet port and restricting flow [4], [5]. A silicon nitride layer on the substrate surface prevents actuator shorting when the microvalve is closed. The critical voltage at which electromechanical instability occurs depends on the fluidic pressure created by the flow and the mechanical compliance of the microvalve diaphragm. In normal operation, all microvalves are open, allowing flow through the device. Upon closing, flow rate across the array is proportional to the number of microvalves that remain open. A schematic of the microvalve array conceptual design is presented in Fig. 1.

II. Background

A number of MEMS valve devices have been reported in the literature. Most incorporate a diaphragm that is actuated

Manuscript received May 22, 1998; revised August 17, 1998. This work was supported by the DARPA ASSERT program under Contract DABT63-95-C-0065. Subject Editor, G. B. Hocker.

The authors are with the Department of Aerospace and Mechanical Engineering, Boston University, Boston, MA 02215 USA.

Publisher Item Identifier S 1057-7157(98)09274-9.

to cover or uncover an inlet flow port. Method of actuation, flow path design, and fabrication techniques distinguish the various types.

Terry *et al.* (1978) [6], [7] introduced what was perhaps the first silicon-micromachined microvalve. It was an injection valve in a gas chromatographic air analyzer fabricated on a 2-in silicon wafer. The valve body was anisotropically etched into the silicon wafer in three steps to form the valve cylinder, seating ring, and two through holes. Actuation was achieved with an electrical solenoid plunger. Gas sample injection volumes as low as 5 nl were reported.

A decade later, Park *et al.* (1988) [8] described a constant flow-rate microvalve designed to operate with cerebrospinal fluid. In this device, no electromechanical actuation was used. Disturbances in inlet pressure on the top surface of the diaphragm were balanced by changes in fluidic pressure on the bottom surface consequently maintaining a constant flow rate through the device. Fabrication steps included bulk silicon etching and silicon-to-glass electrostatic bonding. Flow rates up to 0.1 ml/min were obtained for a pressure differential of approximately 40 kPa.

In the following decade, many micromachined valve systems were reported in the literature by Huff *et al.* (1990 and 1992) [9], [10], Jerman *et al.* (1990) [11], and Trah *et al.* (1993) [12], and the first commercially available microvalve system was produced based on thermal-pneumatic actuation of a single valve.[1]

The first microvalve array system reported in the literature was proposed by Ohnstein *et al.* (1990) [13]. The device was integrally fabricated on a silicon wafer by a sequence of thin-film depositions and consisted of an array of single-cantilever electrostatic actuators positioned over inlet ports anisotropically etched in a silicon substrate. Flow control was achieved by applying a voltage between the actuator diaphragm and substrate. Pressure-flow characterization in open position indicated flow rates up to 700 ml/min of air for a pressure differential of 100 kPa. Closing voltages of 30 V were required for a pressure differential of approximately 15 kPa and a flow rate of 130 ml/min. A leakage rate of 4 ml/min was observed with all the microvalves closed. Individual microvalves could not be addressed independently.

The concept of microvalve arrays was again explored by Bousse *et al.* (1996) [14]. The objective was to interface the microvalve array with a sensing chip in order to improve time response and reduce sample volume. Densities of up to 16 valves/cm^2 were obtained. To generate large actuation forces, the use of a spin-coated silicon–rubber elastomeric pneumatically actuated diaphragm was proposed. For a fixed pressure differential of 30 kPa, liquid flow rates as high as 3 ml/min were reported. Depending on the diaphragm thickness, closing pressures higher than 80 kPa were required.

The single-channel microvalves that represent most of the research and commercial efforts reported to date were designed to modulate flow by altering the height of a narrow channel in the flow path. Such devices yield inherently nonlinear response, limiting their precision and/or range of operation. In the case of flow control achieved with an array system, the response is linear over a wide range of operating flow rates. Flow rate across the device is proportional to number of microvalves open. Also, the array is fabricated using a one-level polycrystalline-silicon surface-micromachining process combined with a single anisotropic bulk etching process and is both scalable and economical. Finally, because each of the microvalves in the array operates on a binary signal, the entire device is readily interfaced to a simple digital controller.

[1]Redwood MicroSystems, 959 Hamilton Avenue, Menlo Park, CA 94025 USA.

III. Microvalve Array Design and Fabrication

A. Design

Microvalve array size was defined as 5×5. All microvalves in a given array were identical. Microvalve diaphragms were squares and fixed along two sides by anchor supports to the substrate. Diaphragm sizes were chosen as a compromise between mechanical compliance and required closing voltage. Smaller diaphragms are subjected to less out-of-plane residual deformation due to fabrication stresses [15] and are less deformed by fluidic pressure, but require higher closing voltages. Electromechanical characterization of previously designed actuators suggested the use of three lateral dimensions: 300, 400, and 500 μm [3]. In all cases, the diaphragms were composed of a layer of 0.5 μm of silicon nitride positioned between two layers of 0.5 μm of polycrystalline silicon.

Selection of the microvalve gap, i.e., the nominal distance between microvalve diaphragm and substrate, represents a compromise between fluidics and electrostatic. Larger gaps increase the achievable array flow rates, which scale with the third power of the gap [1], [2] at the expense of larger required closing voltages, which scale with the square root of the gap cubed [5]. With an increase in nominal gap, the required closing voltage can reach a breakdown limit that makes electrostatic operation of the microvalve impossible [16]. For the devices reported in this paper, a gap of 5 μm was used. This gap is near the high end of the practical range for electrostatic actuation.

During microvalve operation, air flows across the inlet port and microvalve gap to the microvalve outlet. Using laminar flow theory and a short-orifice model, estimates were made of pressure differential across the inlet port and across the microvalve gap. The inlet port size was selected to ensure that the pressure differential across the port was smaller than one tenth of the pressure differential across the gap. An inlet port size of 80 μm $\times$ 80 μm was found to be acceptable. The port was tapered from 640 μm $\times$ 640 μm on the wafer back side to 80 μm $\times$ 80 μm at the microvalve inlet.

Intervalve spacing of 850 μm on a square grid was used for all arrays. Polycrystalline silicon wires were routed from each individual microvalve diaphragm to bonding pads positioned regularly along the sides of the chip. A typical microvalve array design schematic showing the actuator array, wiring, and wire bonding pads is depicted in Fig. 2.

B. Fabrication

Microvalve arrays were fabricated using a one-level polycrystalline silicon surface-micromachining process combined

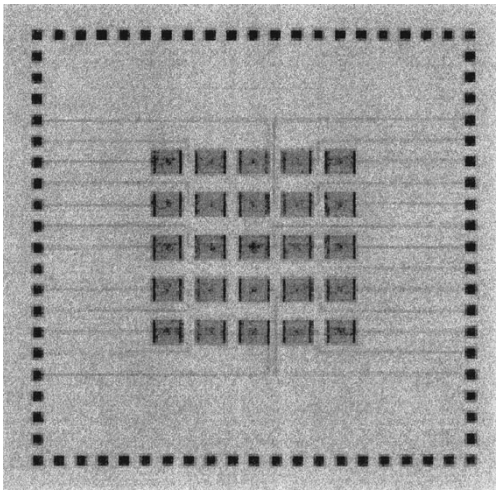

Fig. 2. Typical microvalve array design schematic showing the actuator array, wiring, and wire bonding pads.

with a single anisotropic bulk etching process. The following layers were deposited, patterned, and etched on a batch of 100-mm-diameter silicon wafers:

Layer	Thickness	Purpose
Silicon Nitride	0.5 μm	electrical insulation between diaphragm and substrate
Polycrystalline Silicon	0.5 μm	micro-valve sealing ring
Silicon Dioxide	5 μm	sacrificial layer
Polycrstalline Silicon	0.5 μm	micro-valve diaphragm and wiring
Silicon Nitride	0.5 μm	
Polycrstalline Silicon	0.5 μm	
Metal	0.5 μm	bonding pads

Subsequent to surface micromachining, the back side of each wafer was patterned and etched in potassium hydroxide, followed by reactive ion etching, also from the back side, to remove the silicon nitride layer at the upper end of the anisotropically etched holes. Next, the surface-micromachined microvalve diaphragms were released by wet etching the underlying sacrificial oxide layer in hydrofluoric acid. The resulting structure consisted of a tapered inlet port through the substrate, terminating under the microvalve diaphragm. In the proposed fabrication method, the inlet port size will depend on wafer thickness, mask misalignments, and errors in the crystallographic orientation of the wafer. The final dimension of the inlet port was approximately 100 μm $\times$ 100 μm as measured under a differential interference contrast microscope. Larger inlet ports permit microvalve operation at higher flow rates, but require higher closing voltages due to the pressure field over the port and the larger contact area between diaphragm and substrate.

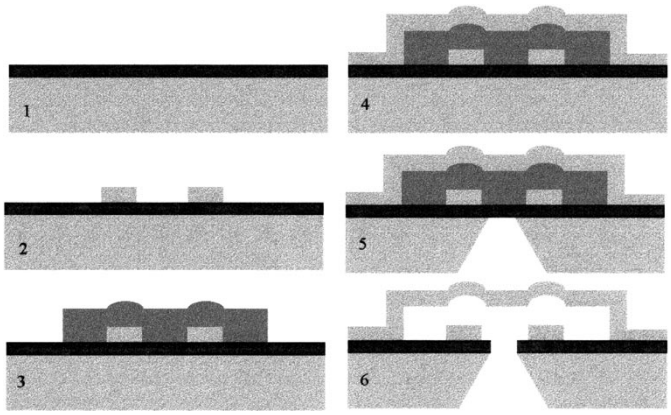

Fig. 3. Microfabrication sequence of a microvalve. Processing steps shown include: 1) base silicon wafer with deposited silicon nitride; 2) deposition and patterning of the first polycrystalline silicon layer to form the microvalve sealing ring; 3) deposition and patterning of the silicon oxide sacrificial layer; 4) deposition and patterning of polycrystalline silicon, silicon nitride, and polycrystalline silicon layer to form the microvalve diaphragm; 5) anisotropic etching of wafer back side to create an inlet port; and 6) reactive ion etching of the silicon nitride and acid etching of the silicon oxide to release the microvalve diaphragm.

Devices were fabricated at the MEMS foundry at the Microelectronics Center of North Carolina (MCNC). A summary of the microvalve fabrication sequence is shown in the cross-sectional schematic of a single microvalve depicted in Fig. 3.

Fabricated wafers were diced into 10 mm $\times$ 10-mm sections, each of which contained a microvalve array for testing. A photograph of a fabricated microvalve array and an anisotropically etched inlet port are presented in Fig. 4.

IV. Test Station for Microvalve Array Performance Evaluation

The devices were tested experimentally using the test station shown in Fig. 5. Each device was secured with epoxy over a 6.35-mm-diameter through hole drilled in a 64-pin ceramic chip carrier and then wire bonded to the chip carrier pads.

The chip carrier was sealed over a mounting stage using an O ring and a closing plate. The mounting stage featured a flow fitting for connection to the test loop and a pressure port for measurement of the pressure at the back side of the device. The test loop consisted of a pressurized tank connected to the mounting stage through a pressure regulator, manual flow control valve, flow meter (OMEGA FMA1810), and microfilter. Pressure was measured using a high-resolution transducer (OMEGA PX425). The mounting stage provided optical access to the device so that the entire assemble could be mounted on either an Olympus BX60M differential interference contrast microscope or on a Phase Shift Technology MicroXAM-30HR interferometric microscope for measurements of diaphragm deflection during operation.

The system was leak tested by installing a device without through holes onto the chip carrier and pressurizing the system. The system held a constant pressure of 150 kPa, well above levels used for testing, for 15 min. The epoxy seal between chip carrier and microvalve chip was leak tested using a chip without access holes in the back side. Pressures as high as 50 kPa were held constant for over 5 min.

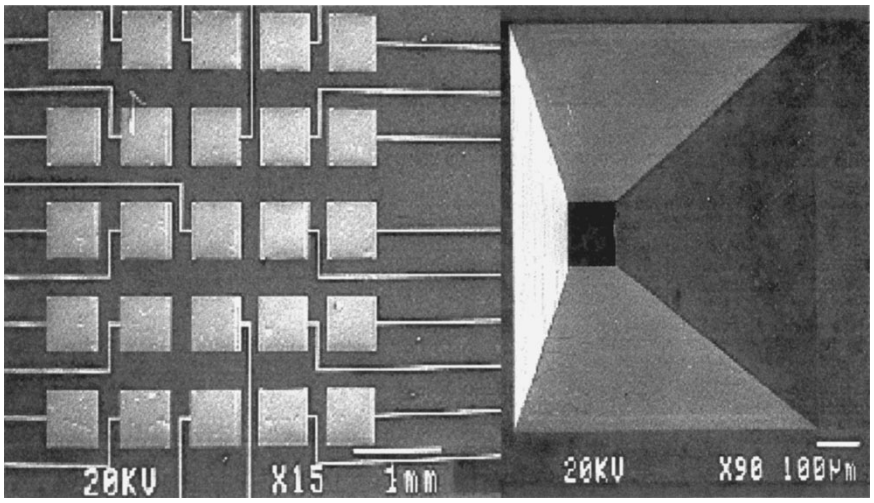

(a) (b)

Fig. 4. (a) Scanning electron microscope (SEM) photograph of the fabricated microvalve array (15X) and (b) an anisotropically etched inlet port (90X).

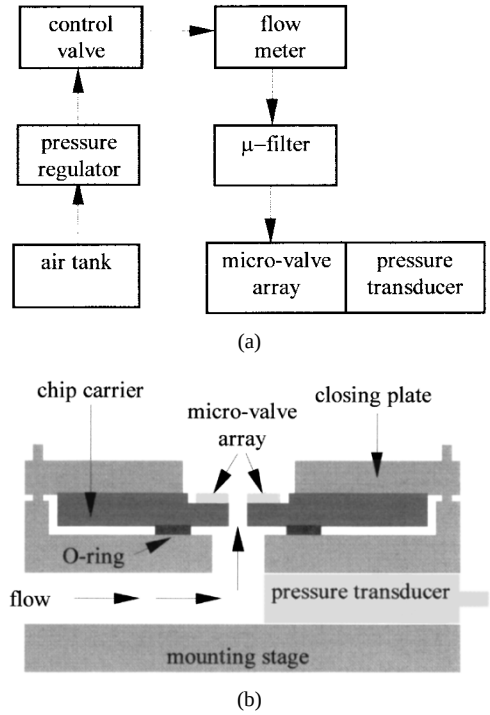

Fig. 5. (a) Microvalve array test station. (b) Microvalve array mounting stage assembly.

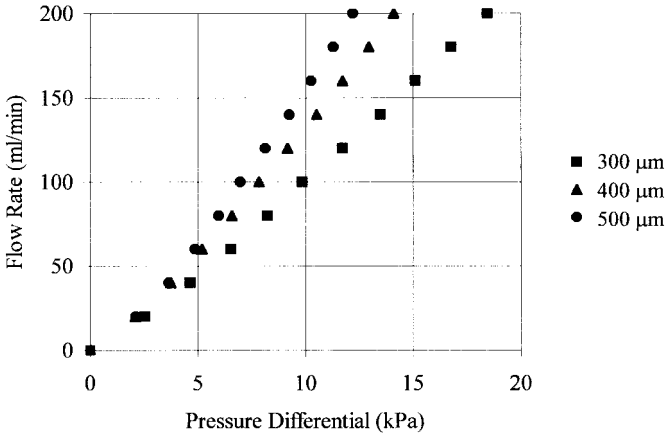

Fig. 6. Flow rate as a function of pressure differential across the microvalve array for fully open arrays for the three diaphragm sizes.

Flow rate as a function of pressure differential across the microvalve array is shown in Fig. 6 for fully open arrays for the three microvalve diaphragm sizes. These results exhibit two notable trends that conflict with expected behavior for low Reynolds number flows [1], [2]. First, the curves exhibit some nonlinearity, with increasing slope at higher pressures. Second, the arrays with larger diaphragms present higher flow rates for a given pressure differential. Both of these trends are a result of diaphragm deflection due to fluidic pressure.

In Fig. 7(a), a surface plot of a 300-μm microvalve diaphragm operating at a pressure differential of 10 kPa is presented to illustrate the degree of deformation due to fluidic pressure. Note that the deflection is nearly two-dimensional (2-D), with little variation in the flow direction. Fig. 7(b) shows the microvalve diaphragm center deflection as a function of pressure differential for the three diaphragm sizes. As expected, the 500-μm diaphragm deforms the most, due to its higher compliance compared to the smaller diaphragms. The results correspond to the average of two measured values.

The linearity of the microvalve arrays was checked by sequentially actuating individual microvalves in the array, while maintaining a constant pressure differential. In Fig. 8, the resulting array flow rate as a function of number of microvalves open for the 400- and 500-μm arrays for a constant pressure differential of 10 kPa is presented. The results clearly demonstrate the linearity of the devices. Also shown in Fig. 8 are linear curve fits for the data, obtained through a linear regression analysis. The 400-μm array exhibits a flow rate of 3.2 ml/min per microvalve at 10 kPa while the 500-μm array exhibits a flow rate of 5.7 ml/min per microvalve at 10 kPa. Also note that the curve-fit equations yield nonzero flow rates with all the microvalves closed, implying leakage. The estimated leakage values are 6.4 ml/min for the 400-μm array and 10.9 ml/min for the 500-μm array, approximately

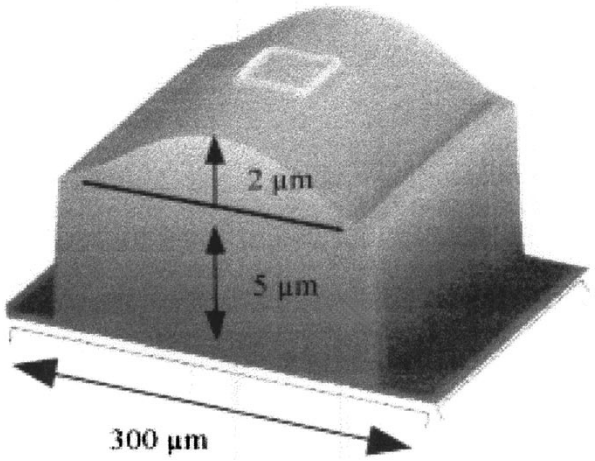

(a)

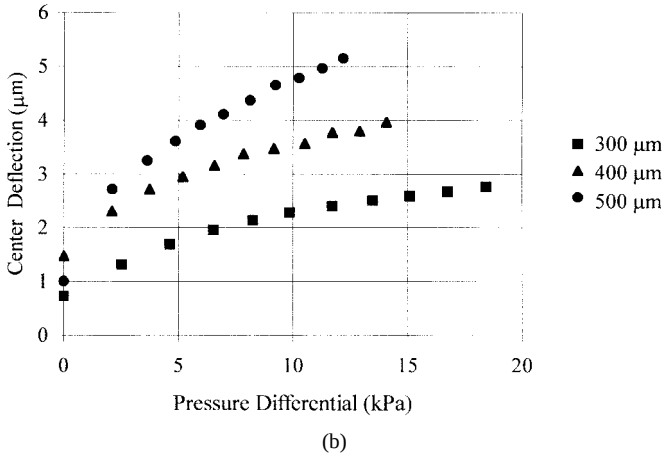

(b)

Fig. 7. (a) Surface plot of a 300-μm microvalve diaphragm operating at a pressure differential of 10 kPa measured using an interferometric microscope. (b) Diaphragm center deflection as a function of pressure differential for the three diaphragm sizes.

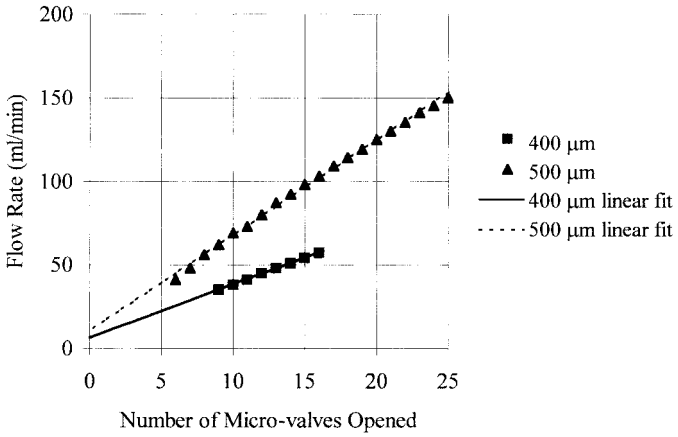

Fig. 8. Flow rate as a function of number of microvalves open for the 400- and 500-μm arrays for a constant pressure differential of 10 kPa.

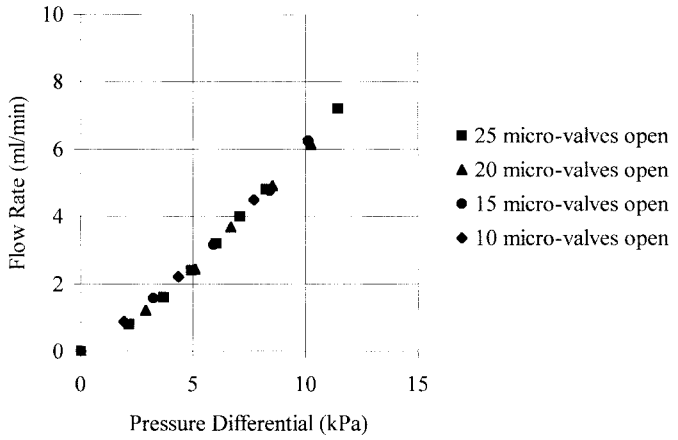

Fig. 9. Flow rate per microvalve as a function of pressure differential for a 500-μm array with 25, 20, 15, and 10 microvalves open.

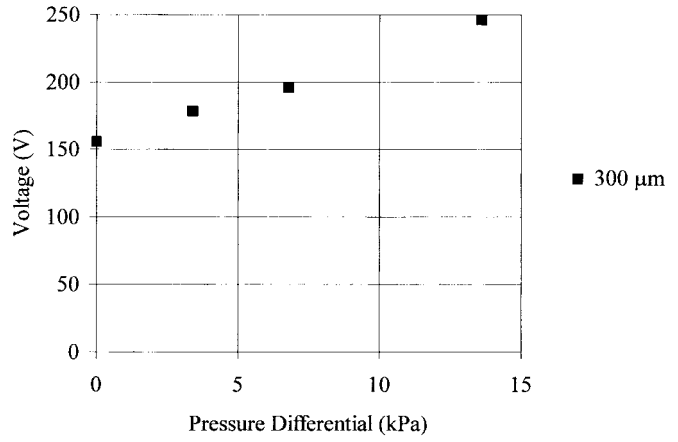

Fig. 10. Closing voltage, corresponding to electromechanical instability, for a 300-μm microvalve as a function of pressure differential.

equivalent to the flow through two open microvalves. These results were obtained for just one device of each size and could not be repeated due to severe electromechanical stiction observed after microvalve closing. The high-leakage values observed are thought to be due to the irregular contact area between diaphragm and substrate upon closing and to the quality of the epoxy seal. To address these problems, diaphragm dimples have been added to future designs and new sealing materials are currently being tested. The presence of dimples will reduce the contact area between diaphragm and substrate generating larger local deformations capable of providing for better sealing characteristics.

To further explore the linearity of the devices, flow rate versus pressure-differential tests were performed on a 500-μm array with 25, 20, 15, and 10 microvalves open. For each test point, the flow rate per microvalve $Q_{\text{micro-valve}}$ was found according to

$$Q_{\text{micro-valve}} = \frac{(Q_{\text{array}} - Q_{\text{leak}})}{N_{\text{open}}} \tag{1}$$

where Q_{array} is the array flow rate, Q_{leak} is the estimated leakage flow rate, and N_{open} is the number of microvalves open. The leakage flow rate is proportional to the estimated leakage flow rate at 10 kPa, $Q_{\text{leak,10kPa}} = 10.9$ ml/min, and to the ratio between the number of microvalves closed N_{closed} and the total number of microvalves in the array. If it is further assumed that the leakage flow rate varies linearly with pressure

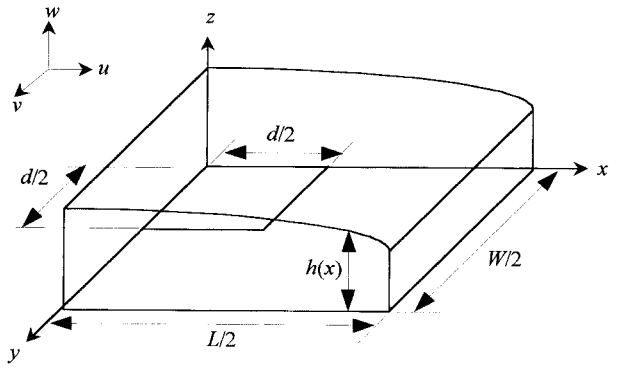

Fig. 11. Geometry and coordinate system used for fluidic model. Symmetry is exploited along the x and y axes, so that only one quadrant of the microvalve is modeled. Coordinate axes in upper left-hand corner show velocity components.

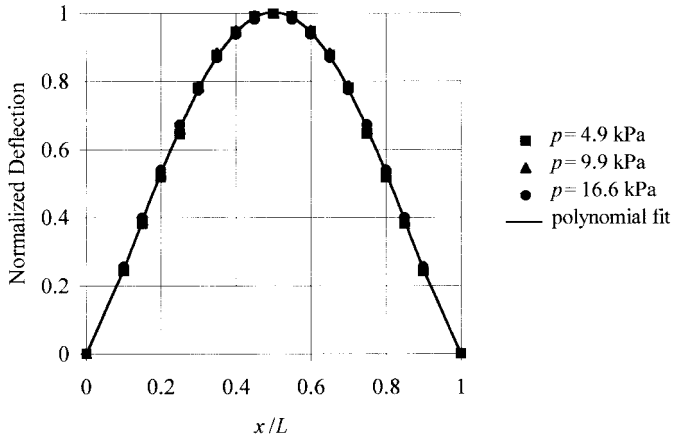

Fig. 12. Diaphragm normalized deflection along center plane ($x = 0$) for a 300-μm diaphragm. Deflection curves are nearly identical for different pressure differentials when normalized by the center deflection.

differential p, it will be given by

$$Q_{\text{leak}} = Q_{\text{leak,10kPa}} \frac{N_{\text{closed}}}{N_{\text{open}} + N_{\text{closed}}} \left(\frac{P}{10}\right). \tag{2}$$

This formulation is only valid under the assumption that leakage occurs primarily through the microvalves and not through the epoxy seal. The results of this analysis are contained in Fig. 9. The curves for the different number of microvalves open coincide well at pressure differentials greater than 5 kPa, confirming linear behavior. At lower pressures, the flow rate per microvalve for 20 and 25 microvalves open are slightly smaller than those for 15 and 10 microvalves opened. This difference may be due to the relative uncertainties associated with the flow-rate measurement. The required closing voltage for a 300-μm microvalve is shown in Fig. 10 as a function of pressure differential. This voltage corresponds to the critical voltage required for electromechanical instability. The closing voltage increases in a nearly linear fashion with increasing pressure differential, due to the higher fluidic pressure that counteracts the electrostatic attraction force and to the larger diaphragm deflection that results in a greater effective gap between the diaphragm and substrate.

V. Fluidic Model

A continuum fluidic model based on incompressible low Reynolds number flow theory was developed to further examine the effects of microvalve diaphragm compliance on flow rate and to provide a tool for next generation designs. Fig. 11 displays the geometry used for the model. Note that symmetry was exploited, so that only one quadrant of the diaphragm was modeled.

The flow across the microvalve gap can be modeled using lubrication theory [1], [2]. This is generally a valid approach under the conditions that $\rho V h^2/\mu L \ll 1$ [2], where ρ is the density, V is the average velocity, h is the characteristic gap, μ is the viscosity, and L is the characteristic length of the passage. This criteria is met for the majority of the cases considered in this study, although the value of $\rho V h^2/\mu L$ is on the order of 0.1 for some of the higher flow-rate cases. Rarefaction effects are neglected in the model [17], [18]. The Knudsen number $Kn = \lambda/h$, where λ is the mean free path

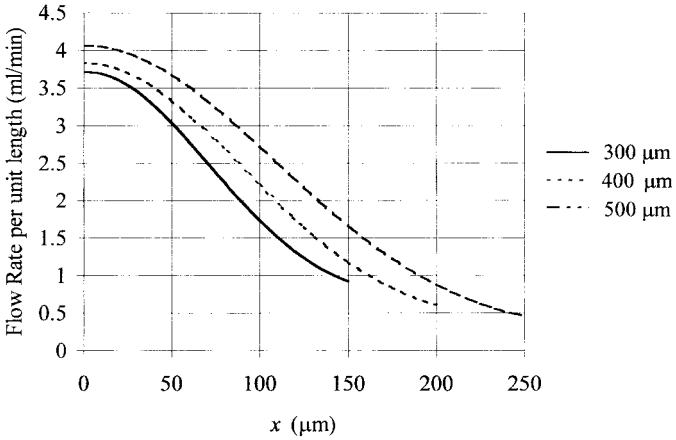

Fig. 13. Predicted flow rate per unit length as a function of x at the microvalve outlet for the three diaphragm sizes at 10 kPa. Total flow rate across a microvalve is four times the area under a given curve.

of the molecules, is approximately 0.01 for the 5-μm gap, which is near the border between continuum-flow and slip-flow regimes [17]. Compressibility effects are also neglected.

The key features of lubrication theory are that inertia forces are small compared to viscous forces and $\partial p/\partial z \approx 0$. Under these conditions, the Navier–Stokes equations can be combined to obtain the Reynolds equation [19]

$$\frac{\partial}{\partial x}\left(h^3 \frac{\partial p}{\partial x}\right) + \frac{\partial}{\partial y}\left(h^3 \frac{\partial p}{\partial y}\right) = 0. \tag{3}$$

Once the pressure field is obtained from the solution of (1), the velocities can be found from

$$u = \frac{1}{2\mu} \frac{\partial p}{\partial x}(z^2 - zh)$$
$$v = \frac{1}{2\mu} \frac{\partial p}{\partial y}(z^2 - zh). \tag{4}$$

The flow rate for a single microvalve can then be found by integrating the v component of velocity across the microvalve outlet

$$Q_{\text{micro-valve}} = 4 \int_0^{L/2} \int_0^h v \, dx \, dz. \tag{5}$$

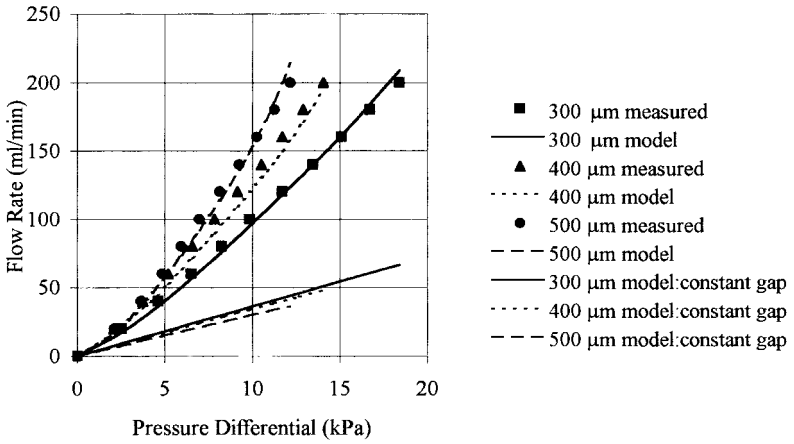

Fig. 14. Predicted array flow rate as a function of pressure differential compared with measured flow rate for the three microvalve diaphragm sizes. Dashed lines are predicted flow rates assuming a constant gap of 5 μm.

The pressure field was estimated from a numerical solution to Reynolds equation using a finite difference approximation with a uniform grid. The boundary conditions on the pressure differential were as follows:

$$\begin{aligned} \frac{\partial p}{\partial x}(x = L/2, y) &= 0 \\ p(x \le d/2, y = 0) &= p_i \\ \frac{\partial p}{\partial y}(x > d/2, y = 0) &= 0 \\ p(x = 0, y \le d/2) &= p_i \\ \frac{\partial p}{\partial x}(x = 0, y > d/2) &= 0 \\ p(x, y = W/2) &= 0. \end{aligned} \tag{6}$$

The second and fourth boundary conditions arise from the assumption that over the inlet port, the pressure differential is constant at p_i, which is assumed to be equal to the pressure on the back side of the microvalve array as measured by the pressure transducer. In all the simulations, the value of the inlet port size was the actual value obtained during fabrication, 100 μm $\times$ 100 μm. Also note that the no-slip condition is not enforced at the solid wall at $x = L/2$. This assumption neglects the presence of a boundary layer along that wall, the thickness of which should scale with the microvalve gap. This should lead to only minimal errors in the prediction of flow rate since the boundary layer spans only a few percent of the area of the flow and since the flow near the end walls is smaller than the flow through the center of the microvalve.

The height of the channel was assumed to be uniform in the y direction and to follow a generic fourth-order polynomial variation in the x direction. The polynomial was obtained by a multiple linear regression of actual measured deflections obtained for a 300-μm microvalve diaphragm. Fig. 12 shows the measured values of diaphragm deflection for three different pressure differentials, normalized by the center deflection. Note that all three cases fall close to the same curve, justifying the approach of using a generic profile. This profile was then used with the measured values of the center deflection, as shown in Fig. 7(b), to provide profiles for various pressure differentials for all three diaphragm sizes. Note that the values of h used in solving (1) are found from $h(x) = g + \delta(x)$, where $g = 5$ μm is the microvalve gap and $\delta(x)$ is the deflection profile found from the generic curve.

Fig. 13 shows the flow rate per unit length as a function of x across the microvalve outlet for the three diaphragm sizes at 10 kPa. Note that the total flow rate across the microvalve outlet is the integral over the length of the flow rate per unit length. It is evident that the flow at the center of the microvalve is larger than the flow at the sides, an effect that is attributable mainly to the larger gap in the center due to the diaphragm deflection.

Fig. 14 shows the predicted flow for a fully open array compared with the measured values. The model agrees well with the measurements, with the predicted values within 10% of the measured values for pressure differentials greater than 2 kPa. For lower pressures, the model underpredicts the measured flow rates by about 15% for all three sizes. The difference is small considering the general deflection profile assumed can be attributed to uncertainties on both the flow rate and deflection measurements. Also shown in Fig. 14 are the predicted flow rates for a constant gap of 5 μm assuming no deflection of the diaphragm due to fluidic pressure. Note that the flow rates for all three sizes are significantly lower than the measured values or the predicted values obtained using the deflection profile. This indicates that the diaphragm deflection is an important factor in determining the flow rate through the devices.

Since measured deflection values were used in the fluidic model, the effects of layer thickness and residual stresses are automatically taken into account. Current modeling efforts are aimed at prediction of the diaphragm deflection shape using structural models based on thin-plate theory [4], [5], [20] so that microvalve performance can be predicted without reliance on measured deflection values.

VI. Conclusions

A MEMS microvalve array for fluid flow control has been developed. The device consisted of a parallel array of surface-

micromachined binary microvalves working cooperatively to achieve linear flow control.

Twenty-five element arrays featuring three different-sized microvalve diaphragms were fabricated and tested. Experiments confirmed that the flow varied linearly with the number of microvalves open over a wide range of pressure differentials. Leakage flow rates were estimated to be approximately the equivalent of two open microvalves. The diaphragm compliance, required for electrostatic actuation, resulted in significant deflections during operation due to fluidic pressure. These deflections greatly affected device flow-rate characteristics. An incompressible continuum-based fluidic model was developed using lubrication theory. The model was capable of capturing the effects of microvalve diaphragm compliance on flow rate, predicting flow rates within 10% over the entire range of flow conditions tested experimentally.

ACKNOWLEDGMENT

The authors are grateful to the staff at the Microelectronics Center of North Carolina for their generous assistance.

REFERENCES

[1] G. Leal, *Laminar Flow and Convective Transport Processes: Scaling Principles and Asymptotic Analysis*. Butterworth–Heinemann, 1992.

[2] H. Ockendon and J. Ockendon, "Viscous flow," *Cambridge Texts in Applied Mathematics*. Cambridge, U.K.: Cambridge Univ. Press, 1995.

[3] T. Bifano, "Micro-electro-mechanical actuators arrays for deformable mirrors," in *Proc. 9th ASPE Annu. Meeting*, Cincinnati, OH, Oct. 2–7, 1994, pp. 145–148.

[4] B. Artz and L. Cathey, "A finite element method for determining structural displacements resulting from electrostatic forces," in *Proc. IEEE Solid-State Sensor and Actuator Workshop*, Hilton Head Island, SC, June 22–25, 1992, pp. 190–193.

[5] P. Osterberg, H. Yie, X. Cai, J. White, and S. Senturia, "Self-consistent simulation of electrostatically deformed diaphragms," in *Proc. IEEE Micro Electro Mechanical Systems Workshop*, Oiso, Japan, Jan. 25–28, 1994, pp. 28–32.

[6] S. Terry, J. Jerman, and J. Agell, "A Gas chromatographic air analyzer fabricated on a silicon wafer," *IEEE Trans. Electron Devices*, vol. ED-26, pp. 1880–1886, Dec. 1979.

[7] K. Petersen, "Silicon as a mechanical material," *Proc. IEEE*, vol. 70, no. 5, pp. 420–457, 1982.

[8] S. Park, W. Ko, and J. Prahl, "A constant flow-rate microvalve actuator based on silicon and micromachining technology," in *Proc. IEEE Solid-State Sensor and Actuator Workshop*, Hilton Head Island, SC, June 6–9, 1988, pp. 136–139.

[9] M. Huff, M. Mettner, T. Lober, and M. Schmidt, "A Pressure-balanced electrostatically-actuated microvalve," in *Proc. IEEE Solid-State Sensor and Actuator Workshop*, Hilton Head Island, SC, June 4–7, 1990, pp. 123–127.

[10] M. Huff and M. Schmidt, "Fabrication, packaging, and testing of a wafer-bonded microvalve," in *Proc. IEEE Solid-State Sensor and Actuator Workshop*, Hilton Head Island, SC, June 22–25, 1992, pp. 194–197.

[11] H. Jerman, "Electrically-activated, micromachined diaphragm valves," in *Proc. IEEE Solid-State Sensor and Actuator Workshop*, Hilton Head Island, SC, June 4–7, 1990.

[12] H. Trah, C. Baumann, C. Doring, H. Goebel, T. Grauer, and M. Mettner, "Micromachined valve with hydraulically actuated membrane subsequent to a thermoelectrically controlled bimorph cantilever," *Sens. Actuators A, Phys.*, vol. 39, pp. 169–176, 1993.

[13] T. Ohnstein, T. Fukiura, J. Ridley, and U. Bonne, "Micromachined silicon microvalve," in *Proc. IEEE Micro Electro Mechanical Syst. Workshop*, Napa Valley, CA, Feb. 11–14, 1990, pp. 95–98.

[14] L. Bousse, E. Dijkstra, and O. Guenat, "High-density arrays of valves and interconnects for fluid switching," in *Proc. IEEE Solid-State Sensor and Actuator Workshop*, Hilton Head Island, SC, June 3–6, 1996, pp. 272–275.

[15] P. Krulevitch, "Micromechanical investigations of silicon and Ni-Ti-Cu thin films," Ph.D. dissertation, Univ. Calif., Berkeley, 1994.

[16] J. Cobine, *Gaseous Conductors*. New York: Dover, 1958.

[17] E. Piekos and K. Breuer, "Numerical modeling of micromechanical devices using the direct simulation Monte Carlo method," *J. Fluids Eng.*, pp. 464–469, Sept. 1996.

[18] A. Beskok, G. Karniadakis, and W. Trimmer, "Rarefaction and compressibility effects in gas microflows," *J. Fluids Eng.*, pp. 448–456, Sept. 1996.

[19] R. Panton, *Incompressible Flow*, 2nd ed. New York: Wiley, 1996.

[20] S. Timoshenko, *Theory of Plates and Shells*, 3rd ed. Boston, MA: PWS-KENT, 1990.

Nelsimar Vandelli received the B.S. degree in mechanical engineering from the Military Institute of Engineering, Brazil, in 1986.

He is currently a Graduate Research Assistant in the Department of Aerospace and Mechanical Engineering, Boston University, Boston, MA, and a MEMS Design Engineer for Etalon, Inc./Iridigm Display Corporation, Boston. He was a Mechanical Engineer for the Brazilian Petroleum Company from 1987 to 1992. His initial research included the study of crack propagation using molecular dynamics and the dynamic modeling of ballistic textile composites. He taught the undergraduate course "Mechanics of Materials" in the summers of 1994 and 1995. His current research is focused on the modeling, design, and testing of surface-micromachined electrostatic actuators and deformable mirrors for adaptive optics applications and surface-micromachined microvalve arrays for high-precision flow control.

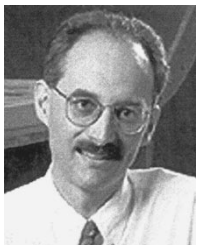

Donald Wroblewski received the B.S. degree in mechanical engineering from Pennsylvania State University, University Park, and the M.S. and Ph.D. degrees from the University of California, Berkeley.

He is an Associate Professor in the Department of Aerospace and Mechanical Engineering, Boston University, Boston, MA. His background encompasses 16 years of experience in thermal-fluids research, including eight years in industry and consulting and eight years in academic research. His current research includes fluid modeling and design of surface-micromachined microvalve arrays for precision flow control and modeling and experiments related to rapid solidification in plasma deposition. His past research focused mainly on fundamental characterization of convection heat-transfer phenomena, including the development and implementation of three-dimensional (3-D) CFD models, with conjugate conduction, for evaluation of electronic chip-cooling techniques.

Dr. Wroblewski was the recipient in 1992 of an NSF Research Initiation Award and Whitaker Foundation Award for Young Investigators.

Margo Velonis received the B.S. degree in aerospace engineering from Boston University, Boston, MA, in 1998. She is currently working towards the M.S. degree in mechanical engineering at the Rensselaer Polytechnic Institute, Hartford, CT.

She is an Aerospace and Mechanical Engineer with the Turbine-Aero Group at Pratt & Whitney, and an Undergraduate Research Assistant at Boston University. She participated in the development of new precision manufacturing technology for compact disc production and implementation of a test station for the characterization of surface-micromachined microvalve arrays for fluid flow control. At Pratt & Whitney, her responsibilities include the analysis, modeling, and aerodynamic design of high-pressure turbine blades for jet engines.

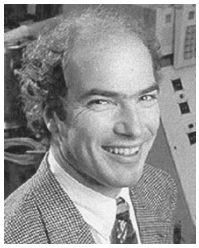

Thomas Bifano received the B.S. and M.S. degrees in mechanical engineering from Duke University, Durham, NC, and the Ph.D. degree in mechanical engineering from North Carolina State University, Raleigh.

He is an Associate Professor in the Departments of Manufacturing Engineering and Aerospace and Mechanical Engineering at Boston University, Boston, MA. He has more than a decade of experience in the fields of precision engineering, optical fabrication, and surface-micromachined systems. As a PI on a nearly completed DARPA-sponsored effort to fabricate MEMS deformable mirrors, he pioneered this new technology and produced the world's first long-stroke continuous membrane active micromirrors. Devices are currently being tested in several DoD applications. His research currently includes the development of micromechanical arrays; basic research on the design, fabrication, and control of new classes of smart materials and systems; development of MEMS-based hydrophonic sensors; and the use of kinetic ion beams to pattern submicrometer-sized features in ceramics. He was selected in 1998 to be one of 100 participants in the National Academy of Engineering's Frontiers of Engineering symposium.

Dr. Bifano has organized and chaired two international conferences for the American Society for Precision Engineering and recently served as a Member of the Board of Directors for that society.